NJC

RSCPublishing

PAPER (or FOCUS or PERSPECTIVE)

Electronic Supporting Information for:

Straightforward Metal-Free Synthesis of an Azacalix[6]arene Forming a Host-Guest Complex with Fullerene C_{60}

Zhongrui Chen,[a] Gabriel Canard,*[a] Cloé Azarias,[b] Denis Jacquemin*[b,c] and Olivier Siri*[a]

[a] *Aix Marseille Univ, CNRS, CINaM UMR 7325, 13288, Marseille, France. Fax: (+33) 491 41 8916; E-mails: gabriel.canard@univ-amu.fr and olivier.siri@ univ-amu.fr.*

[b] *Laboratoire CEISAM, UMR CNRS 6230, Université de Nantes, 2, rue de la Houssinière, 44322 Nantes, France. Email: Denis.Jacquemin@univ-nantes.fr*

[c] *Institut Universitaire de France, 1, rue Descartes, 75231 Paris, France*

Additional theoretical analysis

Conformational search

We assessed the different possible conformations of **3b**. The different optimized structures are displayed in Figure S1 and their relative free energies are reported in Table S1. The most stable conformer corresponds, as expected, to the structure obtained from the crystallographic X-ray analysis. The other conformers show a relative free energy that is larger than 10 kcal.mol^{-1}. Hence, the formation of such energetic conformer is very unlikely at room temperature. This conclusion is valid irrespective of the used theoretical model.

Table S1: Relative free energies (ΔG_{rel} in kcal.mol^{-1}) of the different conformers of **3b** (see Figure S1). SBS and LBS stand for 6-31G(d) and *def2*-QZVP, respectively. PCM and SMD are two solvent models introduced as single-point corrections to the gas phase values here.

Conformer	Gas SBS	Gas LBS	+PCM SBS	+PCM LBS	+SMD SBS	+SMD LBS
(a)	0	0	0	0	0	0
(b)	11	14	15	17	14	17
(c)	36	38	36	38	35	37
(d)	43	46	43	45	41	43
(e)	45	47	44	45	42	43
(f)	47	49	44	46	41	44

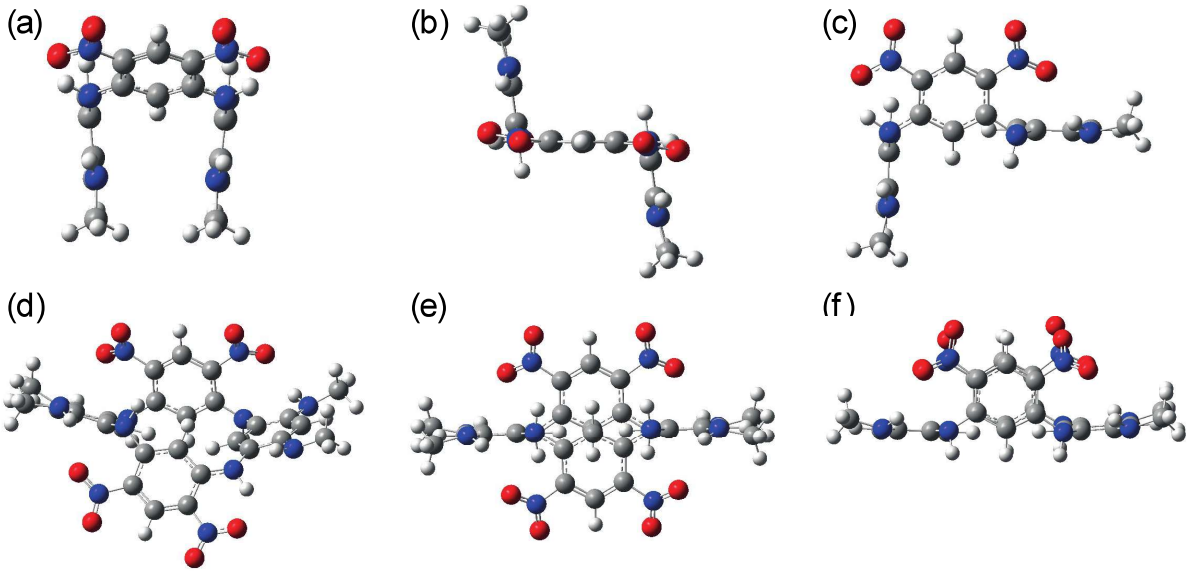

Fig. S1: DFT optimized conformers of **3b**

We also assessed the different possible conformations of **4b.** Despite stating with many different conformers, only three relatively stable were finally obtained. Their structures are displayed in Figure S2 whereas their relative free energies are reported in Table S2. The most stable conformer is found to be perfectly corresponding to the one obtained through XRD. The two other conformers show a relative free energy that is larger than 10 kcal.mol^{-1}. Therefore the conclusions made for **3b** holds: only one conformer should dominate in solution. Note however that these theoretical conclusions have been obtained with simplified structures in which the long alkyl chains were replaced by methyl groups (see computational details). As the most stable structure is rather coiled, we reasoned that the use of the methyl groups to replace the long alkyl chains might be a non-ideal choice. Consequently, we re-optimized the three conformers displayed in Figure S2 replacing the methyl groups with propyl chains. The resulting structures are very similar and their relative energies follow the same trend as in Table S2.

Table S2: Relative free energies (ΔG_{rel} in kcal.mol^{-1}) of the different conformers of **4b** (see Figure S2). See caption of Table S1 for more details.

Conformer	Gas SBS	Gas LBS	PCM SBS	PCM LBS	SMD SBS	SMD LBS
(a)	0	0	0	0	0	0
(b)	13	12	12	10	11	9
(c)	20	17	18	15	16	14

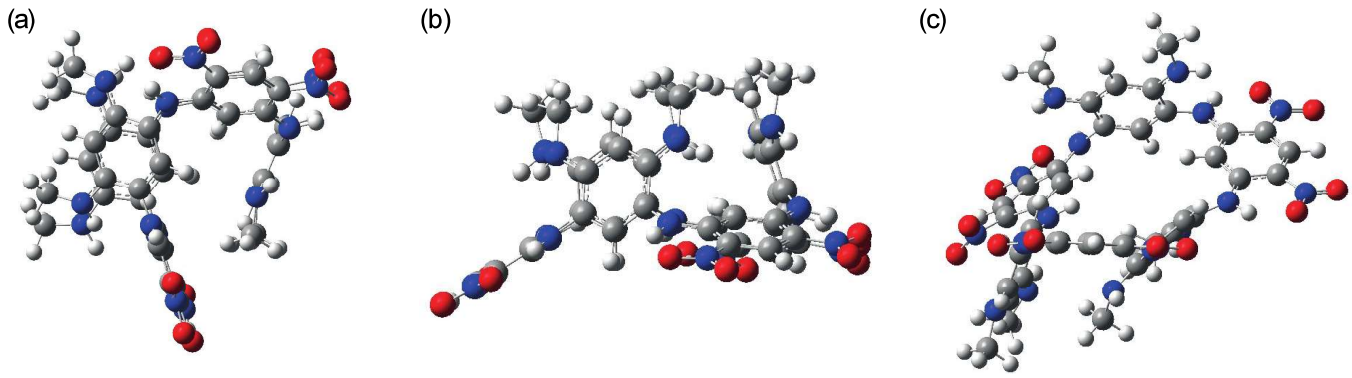

Fig. S2: DFT optimized conformers of **4b**

Simulated NMR spectra

In Table S3, we compare the theoretical and experimental ^{1}H chemical shifts for **3b**. The theoretical chemical shifts are in very good agreement with the NMR measurements, confirming the assignments made in the main text. We note that the largest errors are obtained for hydrogen atoms H_b and N-H_{bridge}, for which theory is overestimating the chemical shifts. This discrepancy can be explained by the fact that these two hydrogen atoms are involved in hydrogen bonds with the oxygen atoms from the nitro group. In the calculations, these bonds are frozen in their optimal geometries, but at room temperature, the groups are vibrating around their optimal positions. In fact, if we compute NMR shifts for a structure in which all the oxygen atoms of the nitro groups have been twisted 45° out of the plane (see Figure S3), we obtain a large difference for the H_b and N-H_{bridge} signals (see Table S3), the experimental values being in between these two extreme situations, as expected. This is a further hint that there are indeed significant H-bonds in **3b**.

Table S3: Experimental and theoretical ^{1}H NMR data in deuterated chloroform for **3b** (see Scheme 1 in the main text for numbering). The values in italics have been obtained with twisted nitro groups (see Figure S3 and text above). All values are in ppm.

Hydrogens	δ_{exp}	δ_{theory}	$\Delta\delta_{(theory-exp)}$
H_a	5.49	5.52 (*5.38*)	0.03
H_b	9.26	9.90 (*8.17*)	0.64
H_c	6.58	6.77 (*6.68*)	0.19
H_d	5.82	5.87 (*5.88*)	0.05
N-H_{bridge}	8.85	9.78 (*6.14*)	0.93
N-H_{ext}	3.91	4.29 (*4.53*)	0.38

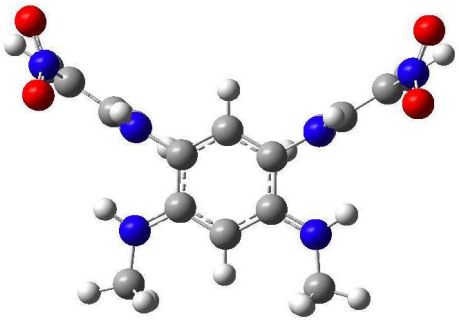

Fig. S3: **3b** structures with nitro group twisted by 45°

In Table S4, we compare the theoretical and experimental ^{1}H chemical shifts for **4b** considering the most stable conformer. As theory considers a frozen structure, different chemical shifts are obtained for "equivalent" protons, and we have therefore determined average values, which would be recorded if several equivalent conformers of **4b** do interconvert rapidly on the NMR timescale. Globally, theory provides results in good agreement with the measurements. In particular, DFT foresees (i) larger chemical

shift when going from **3b** to **4b** for protons H_a, H_b, H_c, N-H_{bridge} and smaller chemical shift for N-H_{ext}, which fits experiment (the only discrepancy concerns H_d), see Table S5; (ii) N-H_{bridge}, H_a and H_c more affected by the extension of the number of phenyl rings than H_b or H_d which also fits the measurements. Again, the largest discrepancy between theory and experiment is obtained for the atoms involved in the hydrogen bonds.

Table S4: Experimental and theoretical ^{1}H NMR data in deuterated chloroform for **4b** (see Scheme 1 in the main text for numbering). All values are in ppm.

Hydrogens	δ_{exp}	δ_{theory}						Aver. δ_{theory}	$\Delta\delta_{(theory-exp)}$
H_a	5.95	6.31	6.31	5.39				6.00	0.05
H_b	9.33	9.95	9.99	10.12				10.12	0.69
H_c	7.05	6.89	7.68	8.11				7.56	0.51
H_d	5.74	5.56	6.09	6.55				6.07	0.33
N-H_{bridge}	9.51	10.27	10.29	10.41	10.57	10.63	10.81	10.50	0.99
N-H_{ext}	3.68	3.65	3.75	3.84	3.99	4.03	4.10	3.89	0.21

Table S5: Comparison between experimental and theoretical changes in ^{1}H NMR chemical shifts when going from **3b** to **4b** data in $CDCl_3$.

Hydrogens	$\Delta\delta_{exp}$ (ppm)	$\Delta\delta_{theory}$ (ppm)
H_a	+0.46	+0.79
H_b	+0.07	+0.12
H_c	+0.47	+0.79
H_d	-0.11	+0.20
N-H_{bridge}	+0.66	+0.72
N-H_{ext}	-0.23	-0.40

TD-DFT simulated absorption spectra

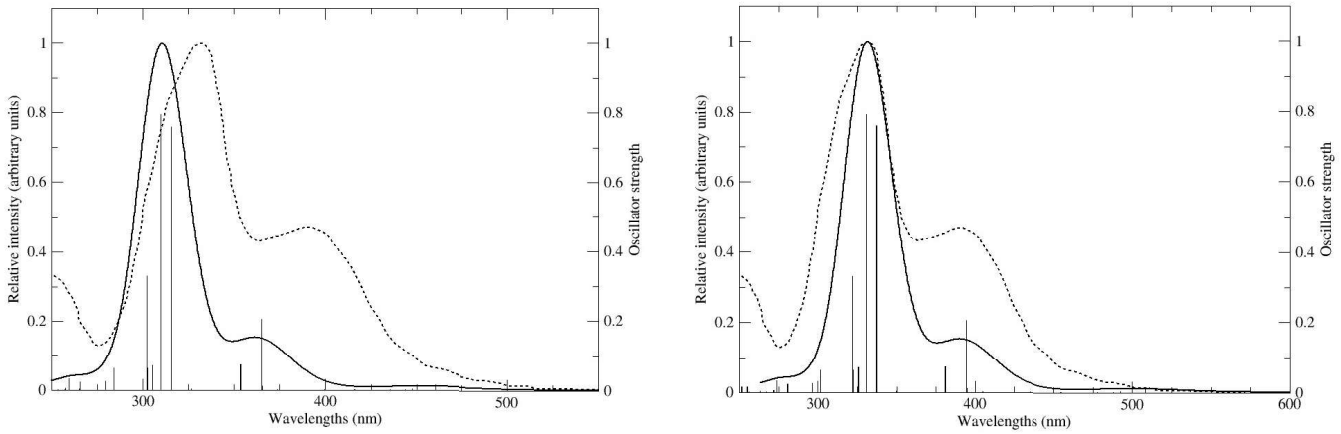

Fig. S4: Comparison between experimental (dotted line) and theoretical (stick and convolution, full line) absorption spectrum of **3b** in $(CHCl_2)_2$. The left panel correspond to the raw TD-DFT values, whereas in the right panel, the theoretical values have been shifted by 0.25 eV to allow more straightforward comparisons with the experiment. The sticks correspond to the TD-DFT electronic excitations and are convoluted with a Gaussian function with a full width at half maximum of 3000 cm^{-1}.

Table S6: Nature of the electronic transitions of **3b** as determined by TD-DFT. We report here transitions with substantial oscillator strength ($f \geq 0.1$) only. H and L stands for the HOMO and LUMO, respectively

Wavelength (nm)	f	Molecular orbital composition
365	0.21	H-7-L (27%), H-6-L+1 (45%), H-4-L+3 (10%), H-3-L+2 (11%)
315	0.76	H-7-L (14%), H-4-L+3 (71%)
310	0.80	H-7-L+3 (23%), H-6-L+2 (73%)
302	0.33	H-7-L+2 (44%), H-6-L+3 (54%)

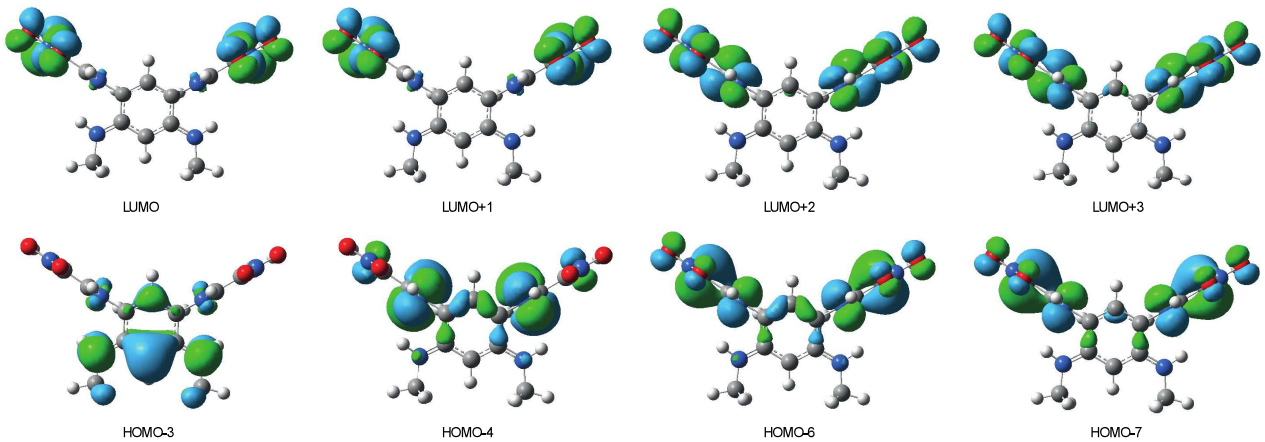

Fig. S5: Key MOs in **3b** (isovalue = 0.02 au)

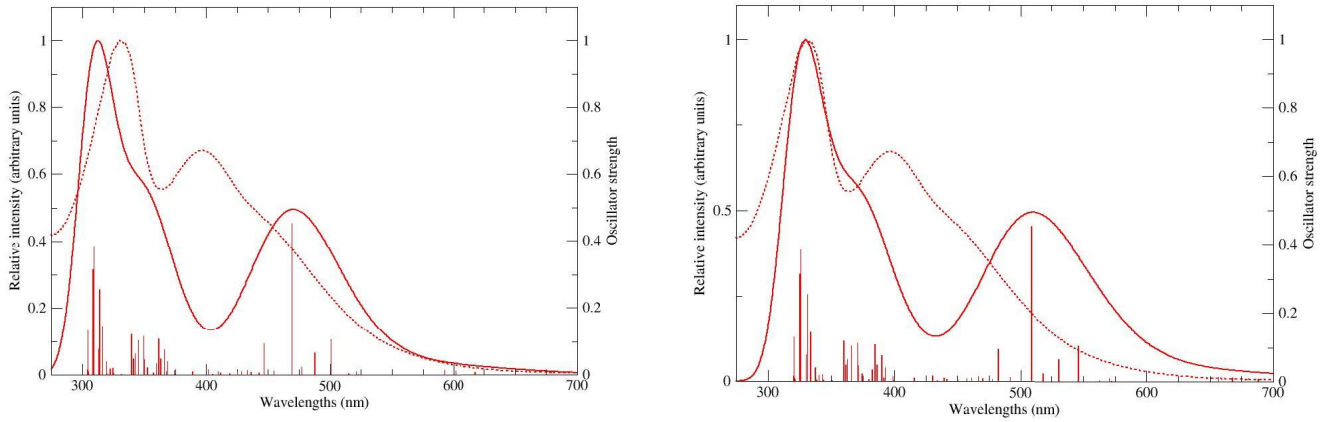

Fig. S6: Comparison between experimental (dotted line) and theoretical (stick and convolution, full line) absorption spectrum of **4b** in $(CHCl_2)_2$. The left panel correspond to the raw TD-DFT values, whereas in the right panel, the theoretical values have been shifted by 0.21 eV to allow more straightforward comparisons with the experiment. The sticks correspond to the TD-DFT electronic excitations and are convoluted with a Gaussian function with a full width at half maximum of 3400 cm^{-1}.

Table S7: Nature of the electronic transitions of **4b** as determined by TD-DFT. We report here transitions with substantial oscillator strength ($f \geq 0.1$) only. H and L stands for the HOMO and LUMO, respectively

Wavelength (nm)	f	Molecular orbital composition
501	0.10	H-L+3 (50%), H- L+4 (43%)
469	0.45	H-1-L+4 (56%), H-L+5 (31%)
362	0.11	H-8-L (20%), H-6-L (24%), H-5-L+3 (11%), H-4-L+3 (17%), H-3-L+3 (13%)
349	0.12	H-7-L+2 (17%), H-4-L+5 (39%), H-3-L+5 (13%)
345	0.10	H-7-L+2 (31%), H-4-L+5 (31%)
340	0.12	H-11-L+1 (11%), H-8-L+1 (28%), H-6-L+1 (14%), H-5-L+4 (11%)
316	0.15	H-8-L+2 (15%), H-6-L+4 (16%), H-6-L+5 (13%)
314	0.26	H-6-L+3 (44%), H-6-L+4 (19%)
309	0.39	H-8-L+4 (13%), H-7-L+3 (12%), H-6-L+5 (12%)
309	0.32	H-10-L+2 (10%), H-8-L+3 (12%), H-6-L+5 (18%)
304	0.13	H-7-L+5 (17%), H-L+7 (21%)

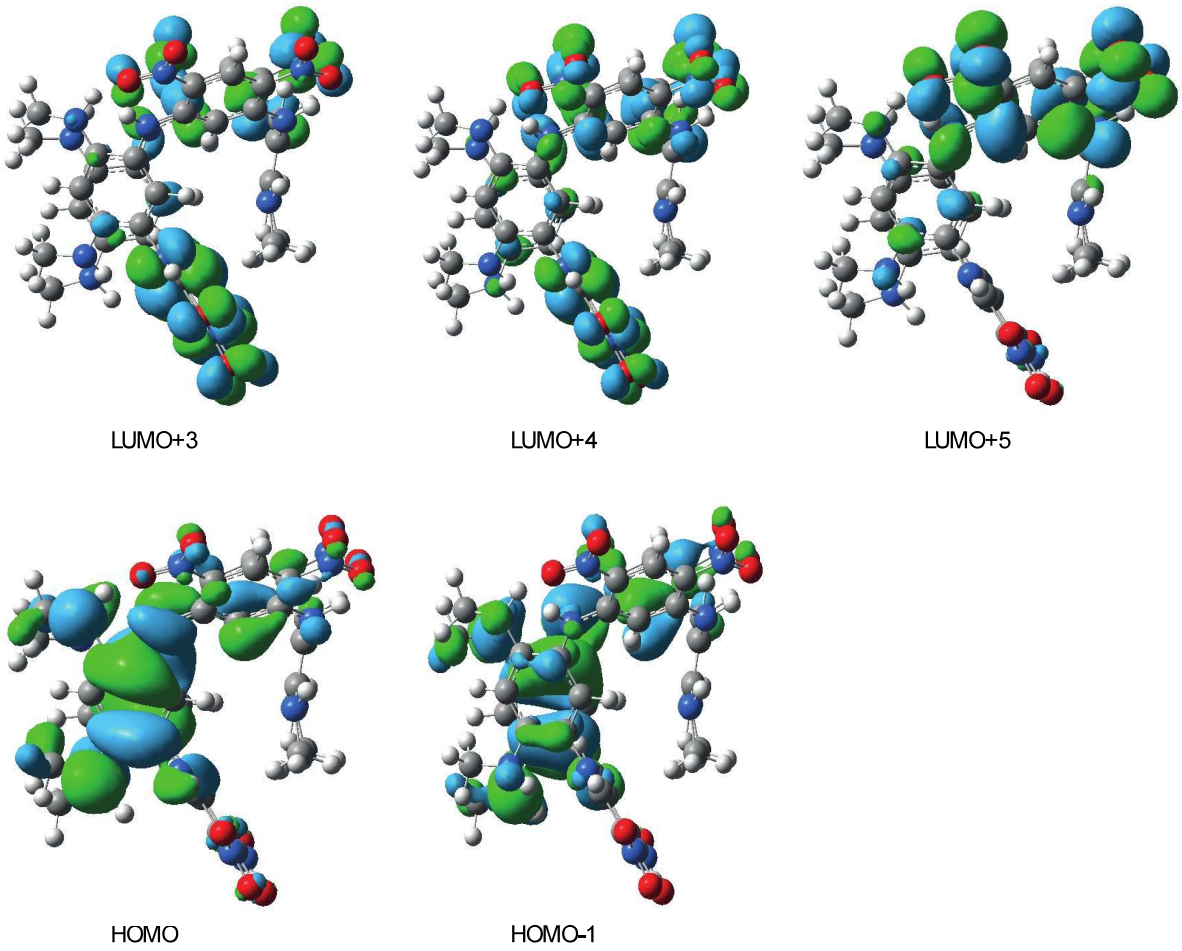

Fig. S7: Key MOs involved in the longest wavelength transition of **4b** (isovalue = 0.02 au)

Complexation with C_{60}: experiment and theory

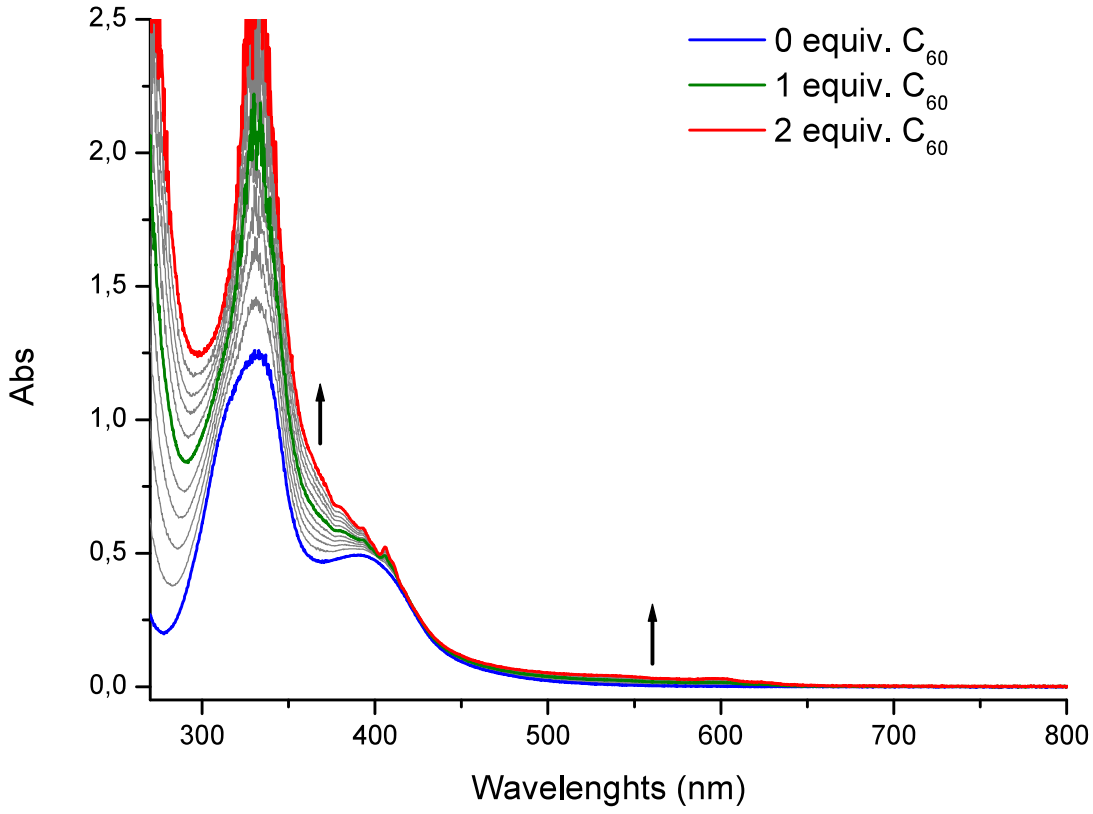

Figure S8. Absorption spectrum of **3b** (4.1×10^{-4} mol.L^{-1}) in the presence of C_{60} in 1,1,2,2-tetrachloroethane at room temperature. The concentration of C_{60} is increasing from 0 to 8.2×10^{-4} mol.L^{-1} (0 to 2 equivalents of C_{60}).

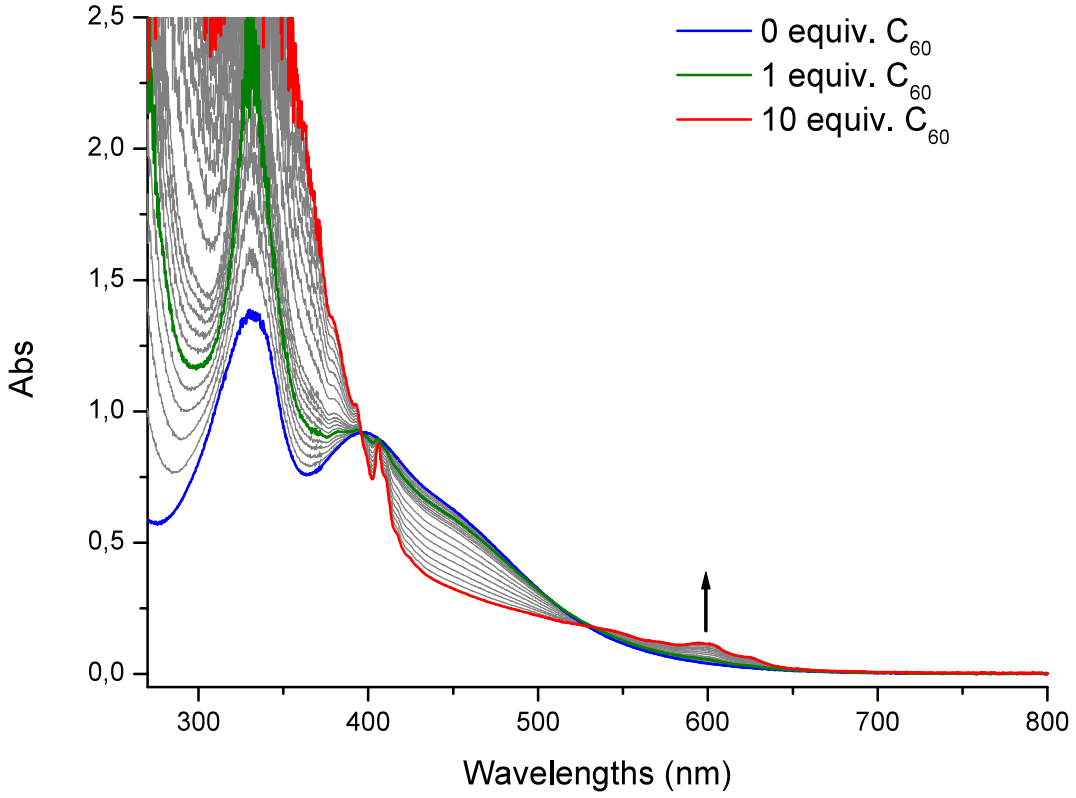

Figure S9. Absorption spectrum of **4b** (4.1×10^{-4} mol.L^{-1}) in the presence of C_{60} in 1,1,2,2-tetrachloroethane at room temperature. The concentration of C_{60} is increasing from 0 to 4.1×10^{-3} mol.L^{-1} (0 to 10 equivalents of C_{60}).

To evaluate the theoretical complexation between **3b** or **4b** and fullerene, we have searched for different complexes using a DFT approach including dispersion corrections. In Table S8, we report the complexation energies determined at various levels of theory for **3b-C_{60}**, the structures being shown in Figure S10. The interaction energies have been computed following a usual procedure, that is optimizing the complexes in gas phase and adding corrections for solvent and basis set effects afterwards. As can be seen, the only complex that presents a stabilising energy when accounting for all effects (rightmost column in Table S8) is (a-1). In this structure the fullerene is interacting with the nitro-bearing phenyl rings. However, the computed complexation energy, ca. -4 kcal.mol^{-1}, remains extremely small.

Table S8: Complexation energies in kcal.mol^{-1} for the complexes found in Figures S10. We provide the complexation total and free energies, determined in gas phase with the small basis set (SBS, 6-31G(d)) and with correction for basis set effects (LBS, *def2*-QZVP) and the impact of solvation (PCM in TCE).

	SBS - Gas		LBS - Gas		LBS - PCM	
	ΔE	ΔG	ΔE	ΔG	ΔE	ΔG
(a-1)	-25	-10	-19	-4	-19	-4
(a-2)	-19	-2	-14	+2	-13	+4
(a-3)	-18	+3	-11	+9	-10	+11

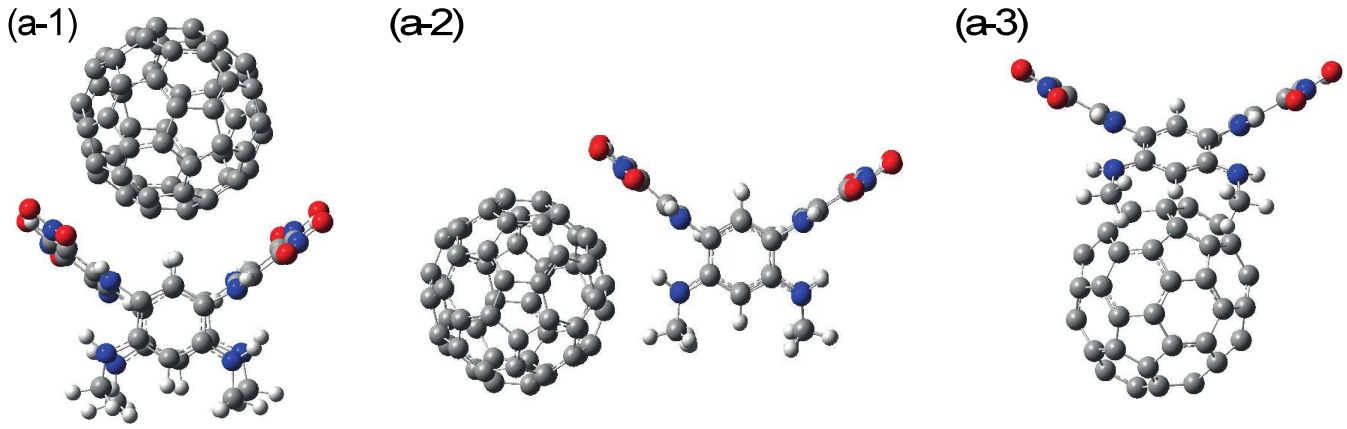

Fig. S10: Theoretical **3b-C_{60}** host-guest complexes.

For the interaction between the fullerene buckyball and **4b**, many different complexes could be identified (see Figure S11 and Table S9). As can be seen, only two out of the seven identified complexes present significantly negative interaction energy: -9 kcal.mol^{-1} for both (a-1) and (b-1). In these two compounds, the C60 is interacting with the nitro-bearing phenyl rings. Interestingly, we note that this interaction takes place with two rings in (a-1) but three rings in (b-1).

Table S9: Complexation energies in kcal.mol^{-1} for the complexes found in Figures S11. We provide the complexation total and free energies, determined in gas phase with the small basis set (SBS, 6-31G(d)) and with correction for basis set effects (LBS, *def2*-QZVP) and the impact of solvation (PCM in TCE). Note that the complexation energies listed below have been determined w.r.t. the corresponding conformer energies listed in Table S2.

	SBS - Gas		LBS - Gas		LBS - PCM	
	ΔE	ΔG	ΔE	ΔG	ΔE	ΔG
(a-1)	-32	-17	-26	-11	-25	-9
(a-2)	-17	-1	-14	+2	-13	+2
(a-3)	-22	-7	-17	-3	-17	-2
(a-4)	+18	+33	+26	+41	+27	+42
(b-1)	-32	-15	-26	-10	-26	-9
(b-2)	-13	+1	-7	+8	-5	+10
(c-1)	-29	-13	-21	-5	-19	-3

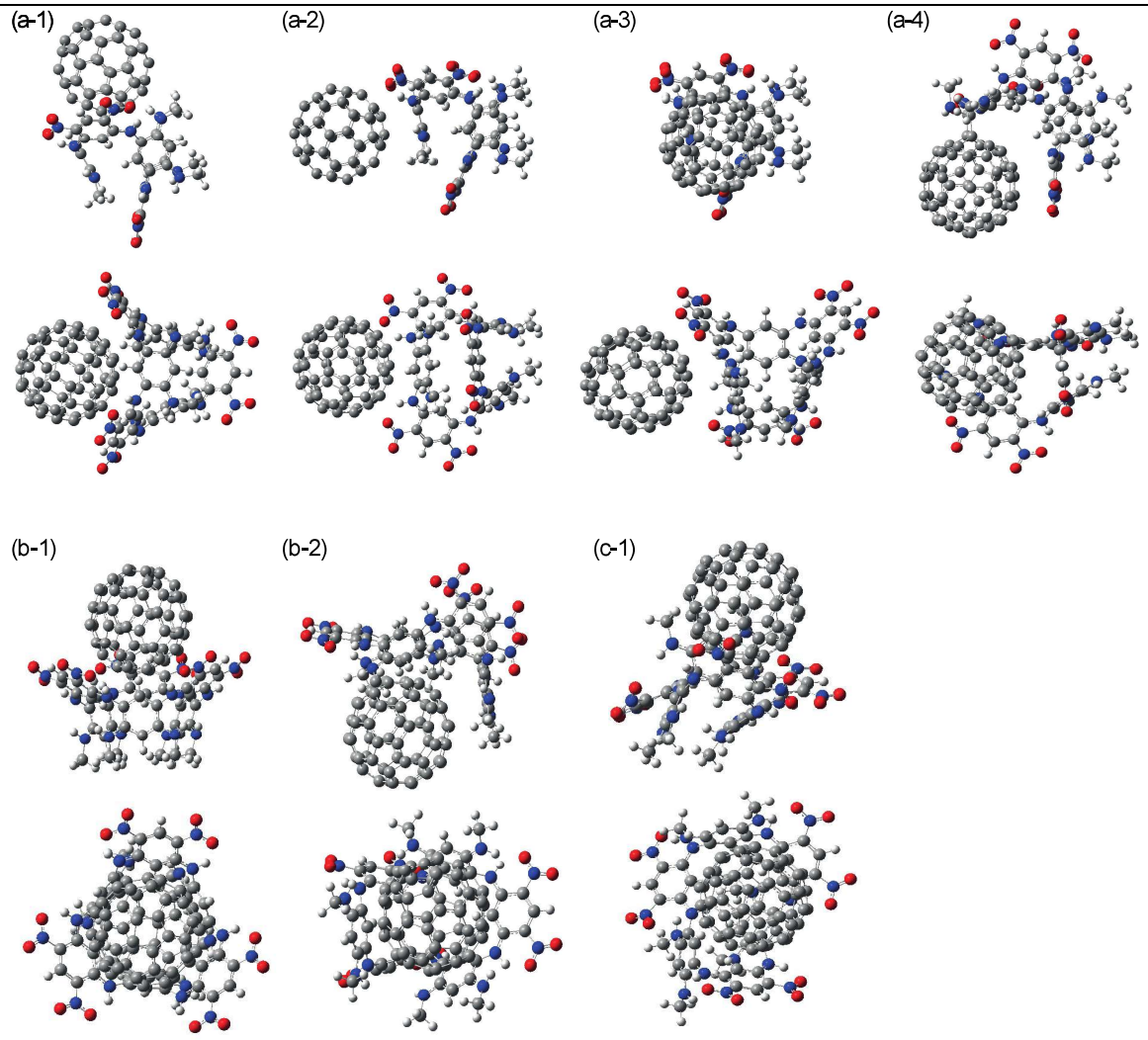

Fig. S11: Theoretical **4b-C_{60}** host-guest complexes (Top and side views for each structure are presented for the sake of clarity).

^{1}H and ^{13}C NMR spectra of 4b and 3b

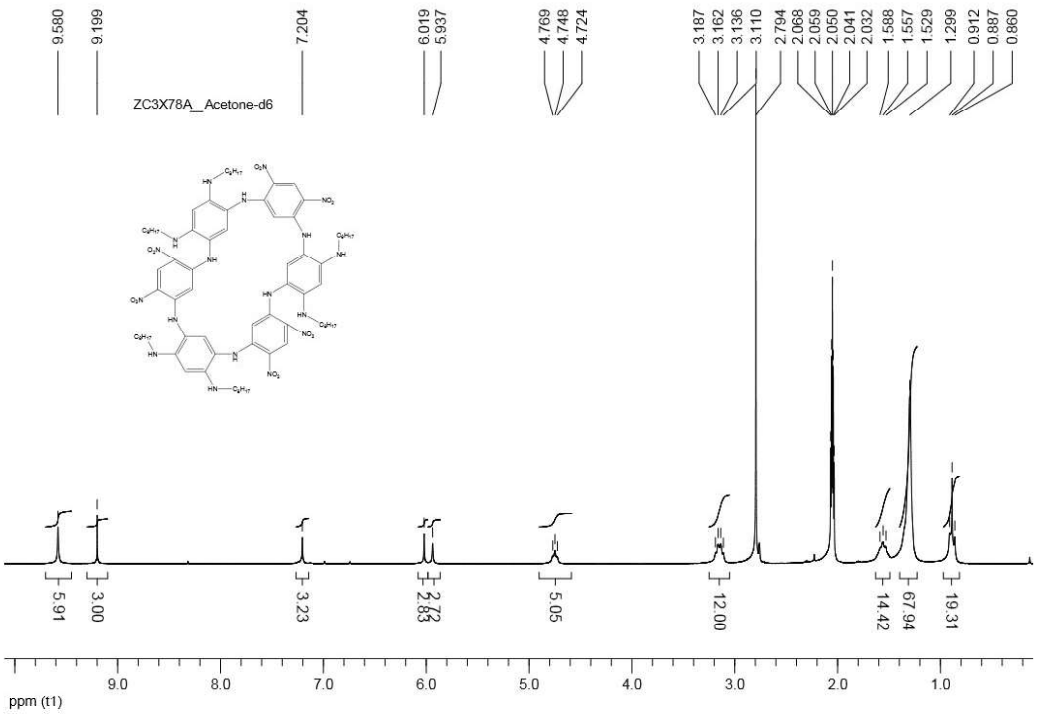

Fig. S12: ^{1}H NMR spectrum of **4b** in Acetone-d_6 (250 MHz)

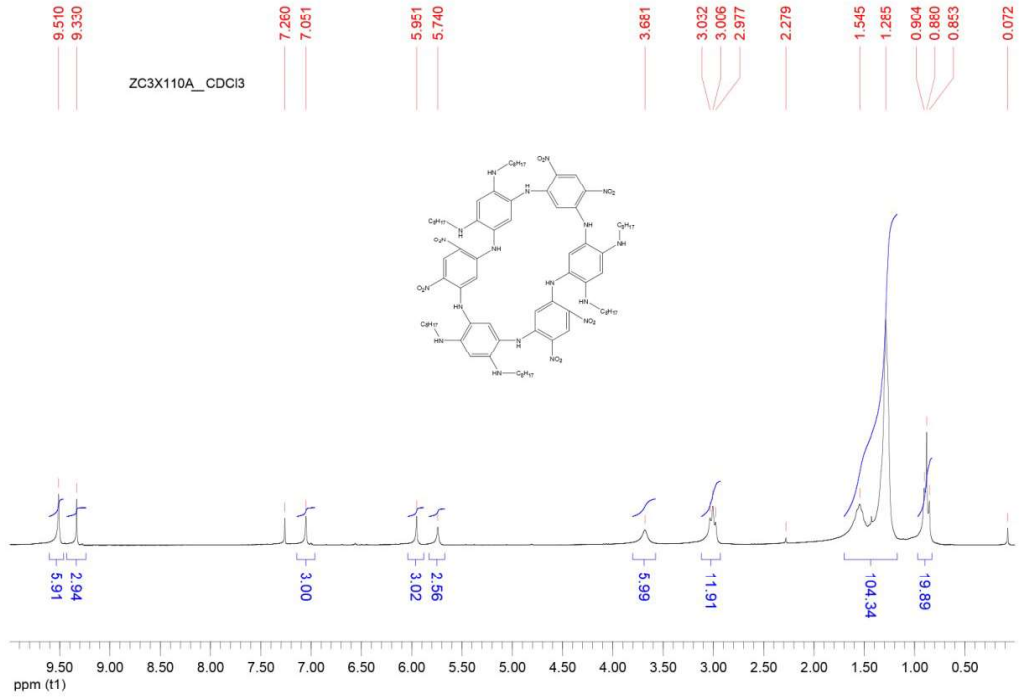

Fig. S13: ^{1}H NMR spectrum of **4b** in $CDCl_3$ (250 MHz)

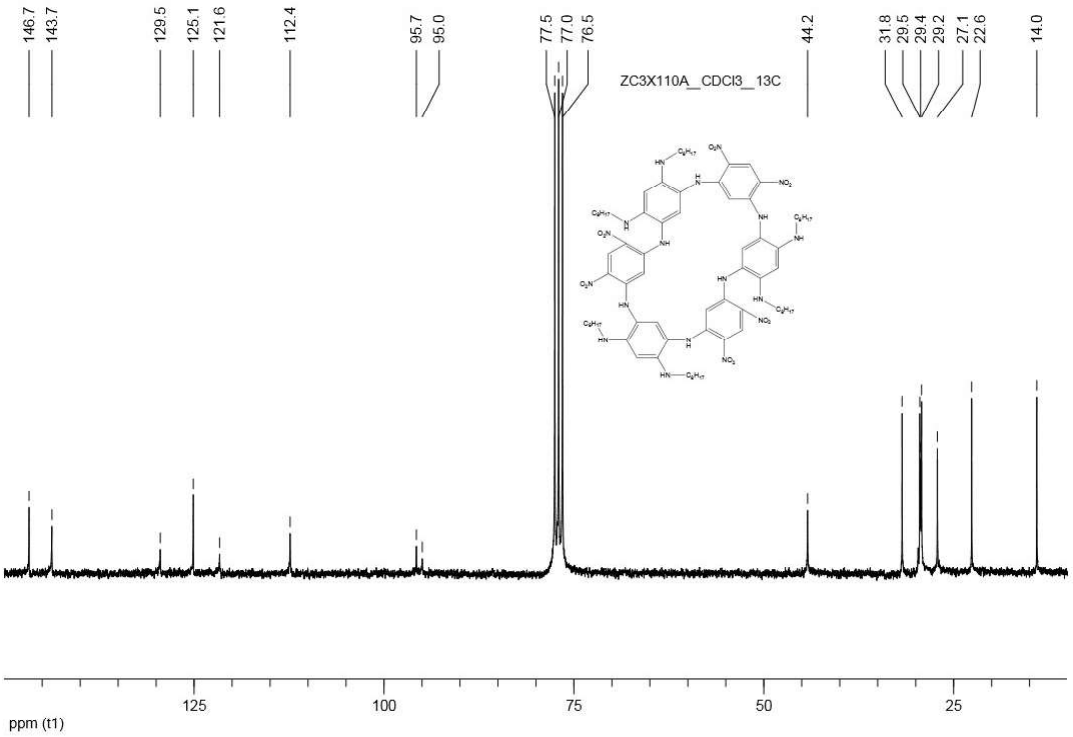

Fig. S14: ^{13}C NMR spectrum of **4b** in $CDCl_3$ (63 MHz)

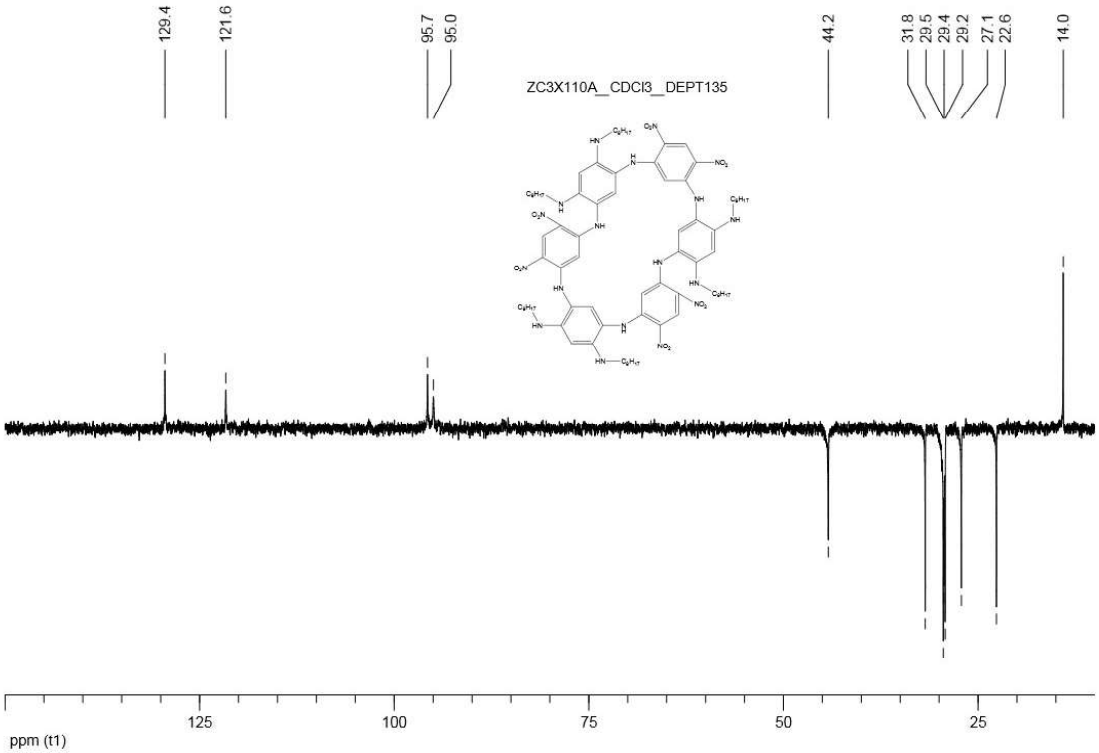

Fig. S15: DEPT135 NMR spectrum of **4b** in $CDCl_3$ (63 MHz)

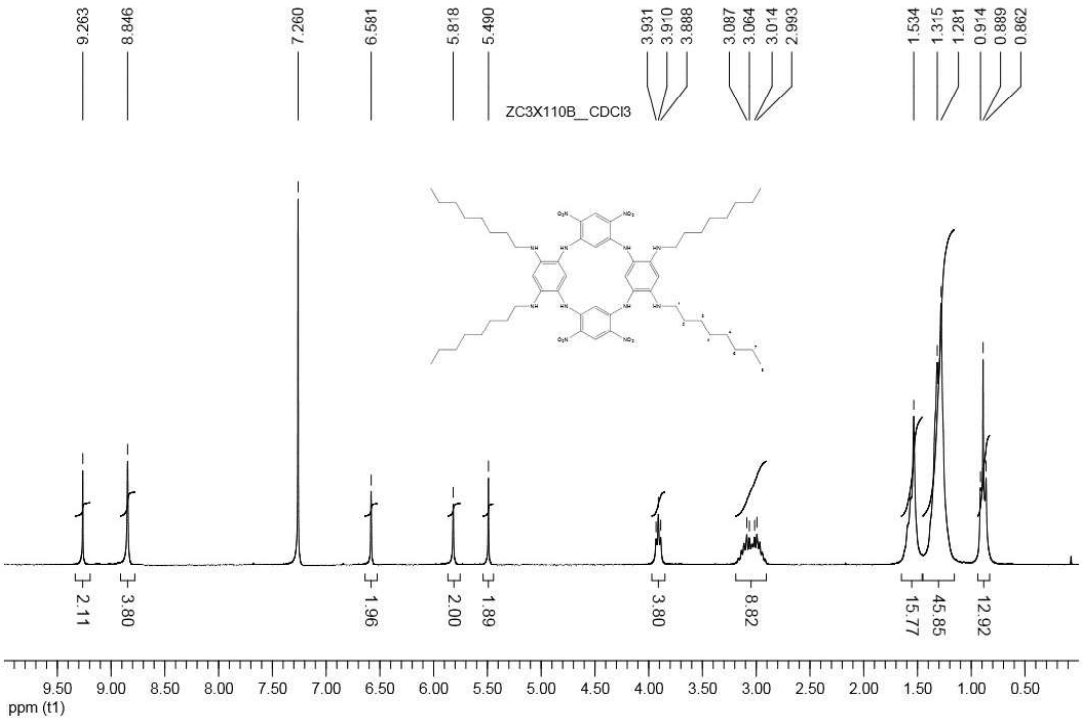

Fig. S16: ^{1}H NMR spectrum of **3b** in $CDCl_3$ (250 MHz)

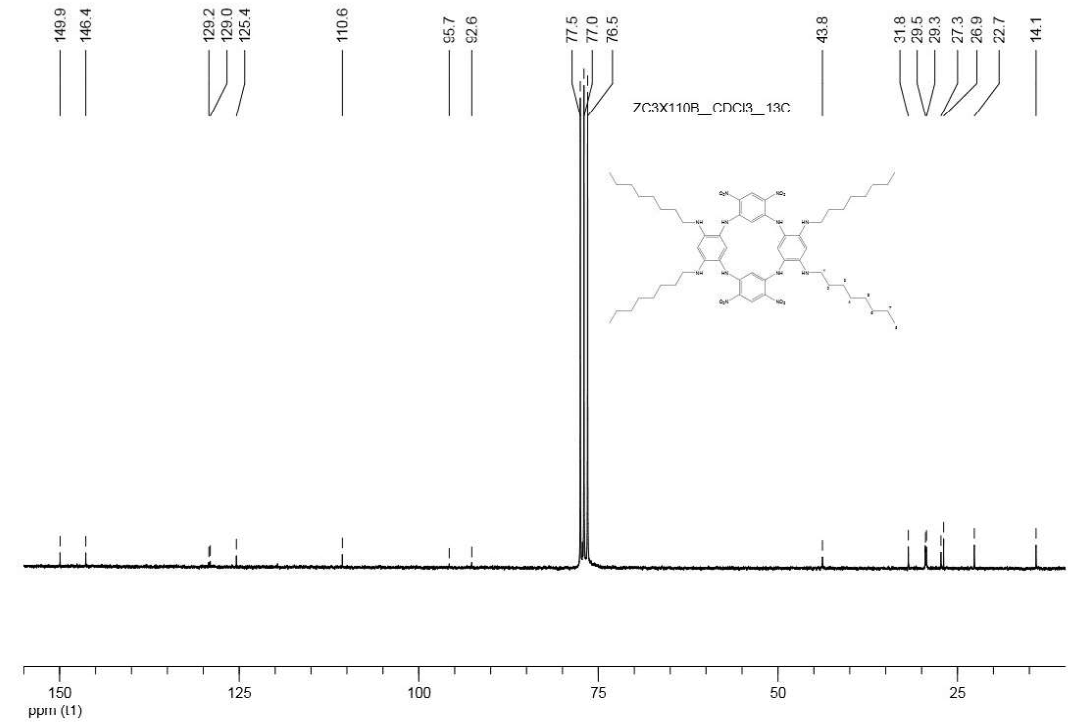

Fig. S17: ^{13}C NMR spectrum of **3b** in $CDCl_3$ (63 MHz)

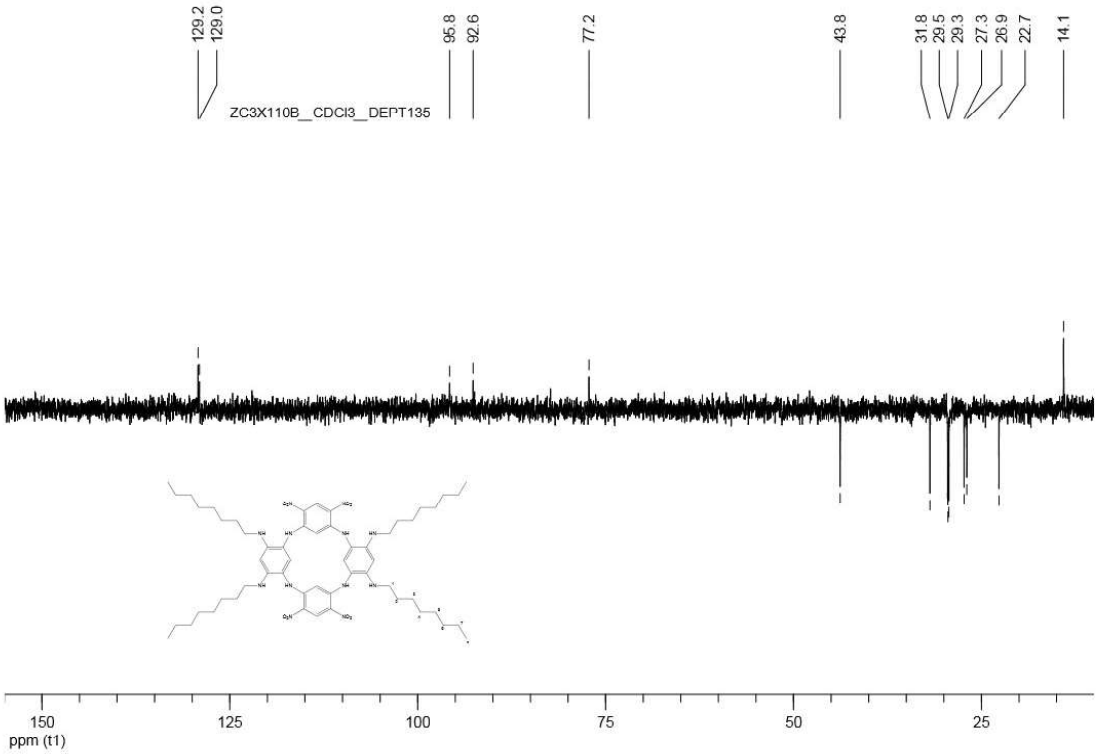

Fig. S18: DEPT135 NMR spectrum of **3b** in $CDCl_3$ (63 MHz)

